

# Adaptive Maximum Torque per Ampere Control of Synchronous Reluctance Motors by Radial Basis Function Networks

Ludovico Ortombina, Fabio Tinazzi, Mauro Zigliotto

**Abstract**—As neodymium and other rare earth materials become a critical commodity, the exploitation of reluctance torque in synchronous motors is certainly an interesting option. Alternative motor topologies span from internal permanent magnet motors to pure reluctance machines. Anyway, any anisotropic structure suffers of some magnetic nonlinearity that call for more sophisticated models to get an efficient torque control. Neural network based algorithms are good candidates for modelling the current-to-flux linkages curves of synchronous reluctance motors, but so far their use was limited by the inherent complexity and the computational burden. This paper proposes the use of a special kind of neural networks, namely, the radial basis function networks, to get the magnetic model of any synchronous motor, including saturation and cross-coupling effects. Through experimental evidence, it will be shown that the structure is light enough to be implemented, trained and self-updated online on standard high-end ac drives. The model is used to track online the maximum torque-per-ampere working point of a synchronous reluctance motor drive.

**Index Terms**—Synchronous reluctance motors, Neural network, Maximum torque per Ampere, Online identification, Motor drives.

## I. INTRODUCTION

As every scientific stream, the control of electrical drives is a system in a dynamic equilibrium among innovative push and technological constraints, with influencing parameters as cost and market demand. Permanent magnet (PM) synchronous motors drives play a key-role in a productive world that requires energy-awareness, reliability, high-performance and cheapness all together. Nevertheless, as far as rare-earth materials become a cost-critical commodity, new constructive topologies appears. Essentially, several motor manufacturers propose the gradual migration from isotropic PM motors to pure synchronous reluctance (SynR) motors. The lack of surface-mounted magnets and of the related equivalent airgap makes the new topologies more prone to iron magnetic saturation and cross-coupling.

Elaborated control techniques aim at exploiting the double torque generation mechanism (PM-based and reluctance) in the most efficient way ever, but they need reliable motor models - especially in case of fractional-slot motors [1]. On the other hand, such models are highly appreciated to give the drive additional self-commissioning and diagnostic features.

The paper has never been presented at conference or submitted previously. L. Ortombina, F. Tinazzi, and M. Zigliotto are with the Department of Management and Engineering, University of Padova, 36100 Vicenza, Italy (e-mail: ludovico.ortombina@studenti.unipd.it; fabio.tinazzi@unipd.it; mauro.zigliotto@unipd.it) *Corresponding author: Mauro Zigliotto.*

The choice of the model is driven by the required degree of completeness. The model can be either simplified by using approximation functions [2] (somewhat loosing accuracy) or tabulate [3] (somewhat loosing resolution). A comprehensive discussion about the existing conventional techniques can be found in [4], [5]. At the end, one may come to the conclusion that the complexity of the interaction in and between the magnetic axes is the ideal application for a black-box approach, which has been proven to accomplish the task in a rather smart way [6].

Actually, the use of artificial neural networks (ANN) in electric drives is not new [7]–[9], even as auxiliary mean for tuning other control techniques, as genetic algorithms [10]. So long, ANNs were considered too demanding for the standard hardware of an electric drive, but nowadays the computational power obtained from the combined use of fast floating point processors and FPGA (field programmable gate array) allows to overcome the obstacle.

A good proof of concept is given by [11], in which a two-degree of freedom PID for the speed control of a PM synchronous motor has been emulated by a neural speed controller, trained online on a high-end ac drive. In that case, the implementation on the laboratory prototype was eased by the adoption of a resilient back-propagation training algorithm, well suited for the application to a linear system and anyway modified on purpose to achieve the astaticism of the controller.

With the same focus on feasibility, the present work is based on the use of a particular class of artificial neural networks, namely the radial basis function (RBF) networks [12]. They use Gaussian curves as activating functions instead of conventional sigmoids and have some local properties which greatly enhance the online update capability, as it will be shown later in the paper. A black-box approach as that offered by RBF networks has proven to be effective and accurate even in case of the highly nonlinear and cross-coupled magnetic model of SynR motors, as detailed in [6]. The limit of that implementation was the complex training algorithm, that made it unsuitable for online implementation. Actually, the magnetic model was accurate, but it had to be necessarily computed offline. This paper proposes a different training algorithm, so that it is possible to exploit the steady state working conditions during the normal drive operations to update (online) the magnetic model of any synchronous reluctance motor, to account for the influence of exogenous and endogenous variables as temperature and ageing, respectively. The RBF training takes just a small portion of time in the lifespan of the SynR motor.

It can be carried out during the very first hours of the entire lifetime span. In this scenario, the RBF network training is a rather cheap price to pay in terms of time.

The result is the on-board availability of a comprehensive and continuously updated model of the relations between currents and flux linkages. Own to the explicit continuous mathematical formulation, the model is well suited for the implementation of advanced energy-savings techniques, as maximum torque-per-ampere (MTPA) or model-based predictive control (MPC), without resorting to any disrupting signal injection. As an effective experimental example, the paper shows the application to the online MTPA point tracking, for the sake of an energy efficient torque control of a SynR motor.

There are several MTPA techniques available in literature, but they can be categorised in two classes, namely the online and offline techniques. The former often requires the adoption of disrupting and continuous signal injection [13], [14] or the use of searching algorithms [15]. The latter are based on offline measurements whose results are stored into look-up tables [16], [17] or implemented for MTPA operation with the aid of polynomial functions [18]. The proposed MTPA technique belongs to the online category for what concern the searching of the MTPA point. However, the classical drawback of these techniques, i.e. the chattering due to the signal injection, is tackled with the aid of the RBF network.

The technique proposed in this paper shares the underlying idea of [6] about the adoption of the AC drive-oriented RBF network for estimating the magnetic flux linkages of a synchronous motor. However, two important innovations are the motivation of this paper. The first one is the study and implementation of a new and lean learning algorithm that enables the online training of the RBF network without any offline operation. The second innovation is the use of the RBF network-based flux linkages to the achievement of the real MTPA condition at any time. In particular, the online implementation of the RBF network yields a true adaptive MTPA-based current control. In the paper, the theoretical background is presented in Sect. II, with a deepening about the local property is given in Sect. II-B. The design of the adaptive RBF network, with the hints for a practical implementation are found in Sect. III and the related paragraphs. The adaptive MTPA tracking algorithm is described in Sect. IV. The practical implementation and validation are reported in Sect. V, with extensive comments and conclusions.

## II. BASICS OF THE RBF-BASED SYNRMOTOR MODEL

Adopting the space vector notation, the torque ( $\tau$ ) and voltage balance equations for a SynR motor in the  $dq$  reference frame fixed to the rotor are the following:

$$\begin{aligned} \mathbf{u}_{dq} &= R_s \mathbf{i}_{dq} + \frac{d\boldsymbol{\lambda}_{dq}(\mathbf{i}_{dq})}{dt} + j\omega_{me} \boldsymbol{\lambda}_{dq}(\mathbf{i}_{dq}) \\ \tau &= \frac{3}{2} p (\lambda_d(\mathbf{i}_{dq})i_q - \lambda_q(\mathbf{i}_{dq})i_d) \end{aligned} \quad (1)$$

where  $R_s$  is the stator resistance,  $\omega_{me}$  is the electric rotor angular speed,  $p$  are the pole pairs and  $\mathbf{u}_{dq} = u_d + ju_q$ ,  $\mathbf{i}_{dq} = i_d + ji_q$ ,  $\boldsymbol{\lambda}_{dq} = \lambda_d + j\lambda_q$  are the stator voltage, current and flux linkages, respectively. Conventionally, the  $d$ -axis is fixed

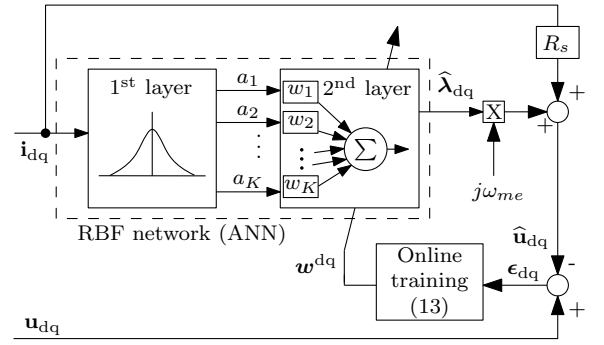


Fig. 1. Motor model based on a RBF network.

along the minimum reluctance path of the rotor and, just this once, all the (nonlinear) dependences on the stator currents are made explicit.

The proposed online identification procedure takes advantage of the *steady state* working periods during the normal operations of the drive. Therefore, for the scope of the present discussion, the (steady state) voltage estimate is simply

$$\hat{\mathbf{u}}_{dq} = R_s \mathbf{i}_{dq} + j\omega_{me} \hat{\boldsymbol{\lambda}}_{dq} \quad (2)$$

without the derivative terms, but with the cross-coupling terms still present. In the following, the main concepts about RBF networks will be briefly recalled, while an in-depth analysis can be found in [6] and [12]. As shown in Fig.1, the flux linkages are estimated by a particular ANN whose weights can be expressed in compact form as a vector of complex numbers:

$$\mathbf{w}^{dq} = [w_1^d + jw_1^q, w_2^d + jw_2^q, \dots, w_K^d + jw_K^q]^T. \quad (3)$$

The weights are updated according to a *training* algorithm that aims at minimising the error  $\epsilon_{dq}$  between the measured and the estimated motor voltage vector:

$$\epsilon_{dq} = \epsilon_d + j\epsilon_q = \mathbf{u}_{dq} - \hat{\mathbf{u}}_{dq} = \mathbf{u}_{dq} - R_s \mathbf{i}_{dq} - j\omega_{me} \hat{\boldsymbol{\lambda}}_{dq} \quad (4)$$

The algorithm requires the a-priori knowledge of a precise and updated value of the stator resistance  $R_s$ , which can be obtained by modern algorithms as for example those described in [19] and [20]. The training algorithm description is reported in Sect. III.

### A. RBF first and second layers

As regards the neural network, a two layer structure, as that depicted in Fig. 1, is suitable for the flux linkages estimation. The first layer was designed to deal with any non-linear input-output behaviour. It is composed of  $K$  Gaussian functions (so called *neurons*) whose centres were regularly spaced in the ( $i_d$ - $i_q$ ) plane. For any given input current vector  $\mathbf{i}_{dq}$  the output of the first layer can be expressed in a compact form as a vector of  $K$  real numbers

$$\mathbf{a} = [a_1, a_2, \dots, a_K]^T. \quad (5)$$

In (5) each Gaussian function is *activated* (i.e. it produces an output) according to the following expression:

$$a_k = e^{-(\|\mathbf{i}_{dq} - \mathbf{g}_k\|_b)^2} \quad (k = 1 \dots K) \quad (6)$$

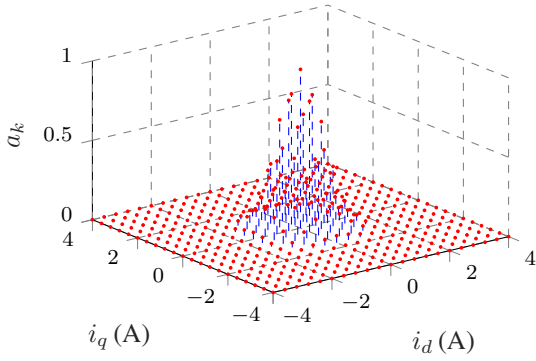


Fig. 2. Local property of the RBF network: components of (5) for  $\mathbf{i}_{dq} = 0$ .

where  $\|\mathbf{i}_{dq} - \mathbf{g}_k\|$  is the Euclidean distance between the  $k$ -th Gaussian centre  $\mathbf{g}_k = g_k^d + jg_k^q$  and the sampled input current vector, and  $b$  is a positive gain whose details are given in Sect. III-B.

The second layer calculates two weighted linear combinations (one for each of the two flux linkage components) of the hidden layer outputs  $a_k$ :

$$\hat{\lambda}_{dq} = \hat{\lambda}_d + j\hat{\lambda}_q = \sum_{k=1}^K a_k (w_k^d + jw_k^q) = \mathbf{a}^T \mathbf{w}^{dq} \quad (7)$$

Substituting (7) in (4) returns the explicit links between the voltage errors and the RBF weights, i.e. the input and the output of the learning algorithm of Fig. 1:

$$\epsilon_{dq} = \mathbf{u}_{dq} - R_s \mathbf{i}_{dq} - j\omega_{me} \mathbf{a}^T \mathbf{w}^{dq} \quad (8)$$

### B. Local property of the RBF network

One of the main reasons for using the RBF networks in online algorithms is the *local property*, which makes  $a_k$  close to zero whenever the input is far enough from the centre  $\mathbf{g}_k$  of the related Gaussian function. As mentioned, this is very useful during the online training, which is performed in a certain steady state condition and not over the entire input range. Thanks to the local property, the update action remains limited to the surroundings of the steady state point, without (badly) influencing the other input regions. It has been found that this simplify the network training, reducing the number of computations. Of course, a complete update needs several local trainings on different steady state points. As an example, Fig. 2 reports the  $a_k$  values, i.e. the output of the RBF hidden layer, calculated with the input  $(i_d, i_q) = (0, 0)$ . It is worth noting that only the Gaussian functions close to the input return a non-zero output.

## III. THE RBF TRAINING AND DESIGN HINTS

The two main features of any neural network are the structure (layers and neurons) and the learning algorithm, i.e. the way a neural network is trained to perform its task. Actually, the learning algorithm is the key-factor, especially in case of an application that requires an online adaptation, as in the present work. Bearing in mind the reduced computational resources in industrial drives, the training should be selected

as computationally light as possible. Although the Levenberg-Marquardt (LM) is the fastest algorithm in the minimisation of nonlinear quadratic problems, and thus can be considered as a standard choice, it brings along heavy computations and it was discarded from the very beginning. Of course, the algorithm heaviness is far less important in case of offline implementations, as it was in [6]. It is important to distinguish between a conventional ANN and the special drive-oriented RBF network proposed in this paper. The former undergoes the conventional training algorithms (for example the back-propagation) that minimise the error iteratively. Conversely, the RBF network allows a direct (non-iterative) computation of the weights update as it will be shown below.

For the design of a computationally efficient learning algorithm it is worthwhile to present a few important considerations:

- As inferable from (6), any current vector measurement  $\mathbf{i}_{dq}$  produces a vector  $\mathbf{a}$  of real numbers. Once substituted in (8), together with the related voltage and speed measurements, it yields an error function whose components  $\epsilon_d$  and  $\epsilon_q$  are linear combinations of the RBF weights  $\mathbf{w}^{dq}$ .
- At steady state (i.e., for a *constant* set of voltage, current and speed vectors), the optimal RBF weights  $\tilde{\mathbf{w}}^{dq}$  are those that bring to zero the error vector (8):

$$\mathbf{u}_{dq} - R_s \mathbf{i}_{dq} - j\omega_{me} \mathbf{a}^T \tilde{\mathbf{w}}^{dq} = 0 \quad (9)$$

The system is clearly underdetermined, since there are  $K$  unknown variables (the weights) and just one equation.

- Given the *local* property of the proposed network (Sect. II-B), the weight set should be updated aiming at improving the flux linkage estimation in the neighbourhood of the considered input only. In other words, it is meaningless to modify the weight linked to a Gaussian far from the present steady state point, since it is not activated (Fig. 2).

The new learning algorithm proposed in this paper aims at changing the existing weight vector  $\mathbf{w}^{dq}$  into  $\tilde{\mathbf{w}}^{dq}$ , so to satisfy the condition (9). One can write:

$$\tilde{\mathbf{w}}^{dq} = \mathbf{w}^{dq} + \Delta \mathbf{w}^{dq} \quad (10)$$

where  $\Delta \mathbf{w}^{dq}$  is the unknown vector to be found. In order to take advantage of the local property of the network and thus reducing the computational efforts, the weight vector is modified using a mask, as shown in Fig. 3. Each dot correspond to a centre  $\mathbf{g}_k$  of a Gaussian function in the  $(i_d, i_q)$  plane. The only weights to be updated will be those related to the Gaussians whose centres falls within the circle centred in the measured  $\mathbf{i}_{dq}$ . This can be obtained by making each weight increment  $\Delta w_k^{dq}$  proportional to the relative activation coefficient  $a_k$ , that is, by imposing

$$\Delta \mathbf{w}^{dq} = \mathbf{W}^{dq} \mathbf{a} = (W^d + jW^q) \mathbf{a} \quad (11)$$

The two unknown real constants  $W^d$  and  $W^q$  can be determined by substituting (10) and (11) in (9) and by solving the equation for  $\mathbf{W}^{dq}$ :

$$\mathbf{W}^{dq} = \frac{\epsilon_{dq}}{j\omega_{me} \|\mathbf{a}\|^2} = \frac{\epsilon_{dq}}{j\omega_{me} \sum_{k=1}^K a_k^2} \quad (12)$$

TABLE I  
APPROXIMATION COEFFICIENTS

$c_5$	$1.06 \cdot 10^{-3}$	$c_2$	$459.3 \cdot 10^{-3}$
$c_4$	$17.64 \cdot 10^{-3}$	$c_1$	$985.9 \cdot 10^{-3}$
$c_3$	$122.1 \cdot 10^{-3}$	$c_0$	$999.2 \cdot 10^{-3}$

Replacing (12) and (11) in (10) finalises the proposed training rule for the RBF network:

$$\tilde{\mathbf{w}}^{\text{dq}} = \mathbf{w}^{\text{dq}} + \frac{\epsilon_{\text{dq}} \mathbf{a}}{j\omega_{\text{me}} \sum_{k=1}^K a_k^2} \quad (13)$$

Every time the ac drive enters in a steady state condition, the voltage error (4) is averaged on a suitable number of measurements, to reduce the possible errors due to spikes and noise, and then the weights of the second layer are updated according to (13).

#### A. Approximation of the Gaussian functions

The online implementation of (13) requires the computation of the exponential functions contained in (5) and the task may exceed the computational power of the drive. Therefore, an appropriate numeric approximation was considered in the present work.

First of all, it is worth noting that the exponents of  $a_k$  in (6) ideally ranges from 0 (when an input exactly matches a Gaussian centre) to minus infinity, when the actual current measurement is infinitely far from the Gaussian centre. Accordingly, the exponentials  $a_k$  range from 1 to 0. In practice, it is reasonable to fix a lower limit  $\xi$ :

$$\xi \leq a_k \leq 1 \rightarrow \ln(\xi) \leq -(\|\mathbf{i}_{\text{dq}} - \mathbf{g}_k\|/b)^2 \leq 0 \quad (14)$$

so that only the exponentials whose exponent is in the range indicated by (14) will be considered for approximation, while the others will be forced to zero. In this work, it was found that a good value was  $\xi = 0.01$ . The generic exponential function was approximated by a 5-th order polynomial, whose coefficients were computed offline by imposing the least mean square error in the range specified by (14):

$$e^x = c_5 x^5 + c_4 x^4 + c_3 x^3 + c_2 x^2 + c_1 x + c_0 \quad (-4.06 \leq x \leq 0) \quad (15)$$

The values of the coefficients are reported in TABLE I. The choice of the order of the polynomial was a trade-off between the required computational power and the mean square approximation error.

#### B. Design hints for the RBF hidden layer

The shape of the Gaussian functions that describe each neuron of the hidden layer, and at large the *local property* of the RBF network, depends on the parameter  $b$  in (6). It also influences the number  $K$  of Gaussian functions, as described in [6]. For the sake of input space completeness, the tighter the Gaussian functions, the higher the number of hidden neurons. The choice of  $b$  can be made so that a Gaussian function gives a negligible contribution ( $a_k$  in (6)) for current vectors whose Euclidean distance from the Gaussian centre is greater than a

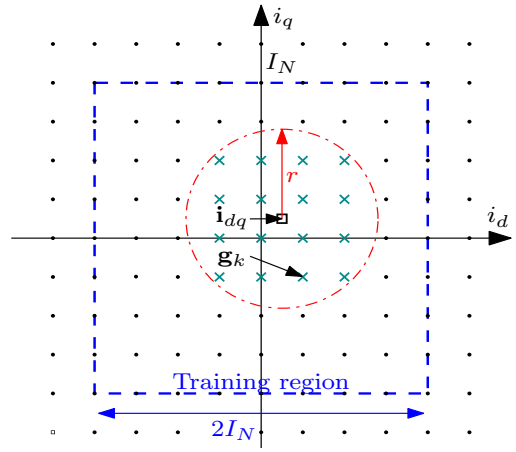


Fig. 3. Example of mask (dotted-dashed line) in the training region (dashed).

design variable  $r$  (Fig.3). In the present work, it was fixed to half of the rated current ( $r = I_N/2$ ). According to (14), this rule of thumb is expressed by

$$b = \frac{\sqrt{-\ln(\xi)}}{r} = \frac{2\sqrt{-\ln(\xi)}}{I_N} \quad (16)$$

In literature, the number  $K$  of hidden neurons is linked to  $b$  and to the side  $I_N$  of the squared training region (Fig.3) by the empirical relation [6], [12]:

$$\sqrt{K} = 4\sqrt{2}I_N b \rightarrow K = -128 \ln(\xi) \quad (17)$$

where the right-hand equation is obtained using (16).

In general, the value returned by (17) is a real number. It is necessary to approximate it to the nearest perfect square, so that the centre of the Gaussian functions will be disposed evenly and symmetrically over the training region, which is a square with side equal to  $2I_N$ . In this paper, as  $\xi = 0.01$ , the number of Gaussian functions was  $K = 576$ . Once  $K$  is set, the coordinates  $\mathbf{g}_k$  of the Gaussian centres in the  $dq$  current plane can be easily derived (Fig. 3).

As a final comment, it is worth noting that all the first layer parameters, i.e. the number of Gaussian functions and their shapes, are chosen during the design phase, while the RBF weights that constitute the heart of the second layer are obtained by online training and adjustment.

## IV. THE MTPA TRACKING ALGORITHM

Substituting (6) in (7) makes clear that the flux linkages estimates are continuous and derivable functions of the stator currents. This is peculiar to the proposed algorithm and quite useful in case of control algorithms that make use of flux linkages derivatives, as in the case of MTPA tracking schemes as that presented hereafter.

For a given reference current vector  $\mathbf{i}_{\text{dq}}^* = I^* e^{j\vartheta^*}$  of fixed amplitude  $I^*$  and variable phase  $\vartheta^*$ , the maximum torque-per-ampere condition is obtained by imposing a null derivative of the torque (1) with respect to  $\vartheta^*$ :

$$\frac{\partial \tau}{\partial \vartheta^*} = \frac{3}{2} p \frac{\partial (\hat{\lambda}_d i_q^* - \hat{\lambda}_q i_d^*)}{\partial \vartheta^*} \stackrel{!}{=} 0 \quad (18)$$

TABLE II  
SYNR MOTOR NAMEPLATE DATA

Nominal current ( $I_N$ )	4 A
Nominal speed ( $\omega_{m,N}$ )	1500 rpm
Nominal Torque ( $T_N$ )	8 N m
Pole pairs ( $p$ )	2
Stator resistance ( $R_s$ )	4.76 $\Omega$
$d$ -axis inductance ( $L_d$ )	380 mH
$q$ -axis inductance ( $L_q$ )	85 mH
DC link voltage	540 V
PWM switching frequency	10 kHz

Substituting  $i_d^* = I^* \cos(\vartheta^*)$  and  $i_q^* = I^* \sin(\vartheta^*)$  and by means of the explicit expression of the flux linkages estimation (7), the condition (18) becomes

$$\frac{3}{2}pI^* \left( \hat{\lambda}_d \cos(\vartheta^*) + \hat{\lambda}_q \sin(\vartheta^*) + \sum_{k=1}^K (w_k^d \sin(\vartheta^*) - w_k^q \cos(\vartheta^*)) \frac{\partial a_k}{\partial \vartheta^*} \right) \stackrel{!}{=} 0 \quad (19)$$

Actually, the  $a_k$  terms, defined by (6), depend on the stator current. Using the polar notation, the derivative of  $a_k$  respect to the current phase angle is

$$\frac{\partial a_k}{\partial \vartheta^*} = 2a_k b^2 I^* (g_k^d \sin(\vartheta^*) - g_k^q \cos(\vartheta^*)) \quad (20)$$

where  $g_k^d + jg_k^q$  is centre of the  $k$ -th Gaussian function in the  $(i_d - i_q)$  plane, as already mentioned above.

Anyway, the straightforward computation of  $\vartheta^*$  might be burdensome. The left-hand term of (19) is greater than zero for current phase angles below the correct one, and vice-versa. Actually, it can be found that the mismatch computed by (19) is proportional to the required current phase angle modification. This is exploited by making the current phase modification proportional to the result of (19). In turn, when the result of (19) is big, the MTPA loci is far. Thus, the angle  $\vartheta^*$  can be modified proportionally to the result of (19). It is worth noting that the online MTPA condition is obtained without *any* disturbing signal injection, as a key-feature of the proposed method.

## V. EXPERIMENTAL RESULTS

The experiments were performed on a SynR motor prototype, whose parameters are shown in TABLE II. The motor was fed by a two-level three-phase IGBT voltage inverter, connected to a variable voltage DC bus and controlled by a fast control prototyping system featuring a dSpace DS1104 controller board, programmed in C-language. The motor phase-to-phase voltages (two out of three) were measured with a custom digital measurement system, based on fast PWM signal oversampling, post-processed by a dedicate FPGA chip.

### A. Validation of the RBF-based flux linkages model

This test evaluates the capability of the proposed RBF network to model the flux linkages of the SynR motor under test. The algorithm requires the measurements of motor voltages and currents, as well as the availability of a precise

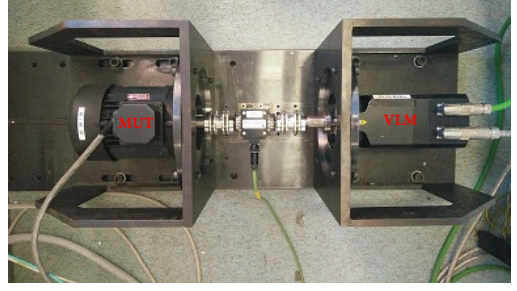


Fig. 4. The SynR motor (left) coupled to a PMSM-based virtual load (right).

value of the stator resistance. The experiment is performed offline, that is, with the SynR motor mounted on a laboratory test bench instead of on a real application. It should be understood that this part is only functional to the validation of the RBF network, while it can be omitted in case of direct implementation on an industrial application. The hardware setup is shown in Fig. 4. The SynR motor was current-controlled in the synchronous  $d, q$  reference frame, and rigidly coupled to a speed-controlled load motor. A torque transducer provides an accurate measurement of the transmitted torque.

The RBF weights training procedure starts by the acquisition of voltages, currents and speed measurements at each steady state condition, followed by the training algorithm (13). Since the training procedure is carried out during steady state condition, the updating of the RBF weights is suspended during transients. However, the torque and current control use the MTPA curve "as it is", i.e. as trained up to the moment in which the transient starts. The two procedure (MTPA adaptation and torque control) do not interfere each other. The current references to the SynR motor drive were generated in correspondence to the crossings of a gridded region in the  $(i_d, i_q)$  plane, as in [6], to cover the whole training region (Fig. 3). The grid resolution was fixed to  $I_N/10$ . The training was performed by the rule (13), with the simplifying assumptions discussed in Sect. III-A.

The validation of the magnetic model was performed by comparison with the benchmark (offline) method [3]. Let the normalised errors be defined by a compact vector notation as

$$\epsilon_N^{dq} = \frac{\hat{\lambda}_{dq} - \lambda_{dqR}}{\max(\lambda_{dqR})} \cdot 100 \quad (21)$$

where  $\hat{\lambda}_{dq}$  are the RBF network estimates and  $\lambda_{dqR}$  are the values obtained by the reference method proposed in [3]. The errors are referred to the maximum value of each flux linkage in the considered working region. The plots of both flux linkages, in case of either null or maximum cross-coupling are reported in Fig. 5, along with the estimation errors, computed according to (21).

The error magnitude remains almost within  $\pm 3.5\%$  for both flux linkages, if one excludes the case  $\hat{\lambda}_q(0, i_q)$  in the low-current range, where it rises up to 7% due to a certain weakness in the RBF network around zero currents. It has been found that this issue can be solved by increasing the number of neurons in the region, in trade-off with the computational burden.



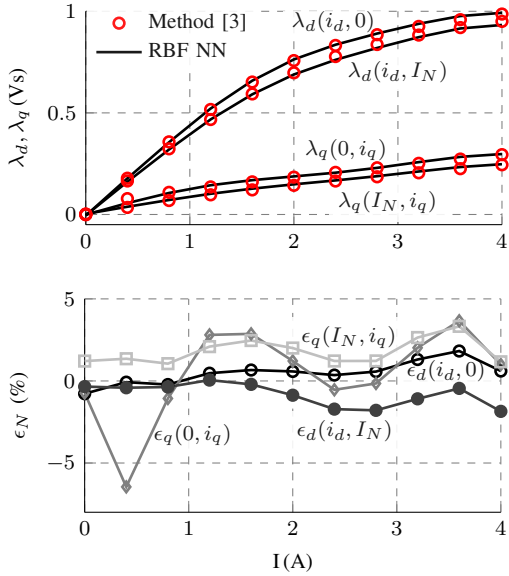


Fig. 5. 2D magnetic maps and relative errors, using [3] as benchmark.

It is also worth mentioning that the benchmark method is of discrete type, i.e. it produces a finite set of values, arranged in a couple of matrix look-up tables (LUTs). On the contrary, the proposed method returns the two-variables *continuous* functions indicated by (7). Therefore, a fair comparison is performed only in correspondence to a finite set of points. Elsewhere, even the benchmark method could introduce errors due to the linear interpolation among points.

It is important to note that the proposed training algorithm is extremely lighter than the one based on the LM algorithm in [6], enabling the implementation on a standard ac drive hardware. It can be found that the time complexity (big O notation) of the LM algorithm is  $O(K^2N)$ , whereas the one proposed in this paper is  $O(K)$ , as inferable from (13). Of course, it is worth reminding that the proposed algorithm needs more iterations to train the RBF network with respect to the LM based algorithm.

The online training feature will be exploited to obtain an efficient MTPA control strategy starting from a blank RBF network. The results are reported in Sect. V-C. In order to accelerate the construction of the fluxes maps, it could also be possible to take advantage of the symmetries and anti-symmetries proper of those functions. The SynR motors magnetic fluxes are anti-symmetric functions of the currents. Therefore, the third quadrant of the  $dq$  current plane is actually the same of the first quadrant, but with opposite sign. The properties of the fluxes and currents relationships help in speeding-up the RBF network training, but they do not alter the concept of the proposed method.

### B. Online RBF training with suboptimal MTPA control

The previous sections have demonstrated the ability of RBF networks to cope with the complexity of the SynR motor nonlinear magnetic model. The training of the network is performed online, exploiting every single steady state condition during the normal drive operations.

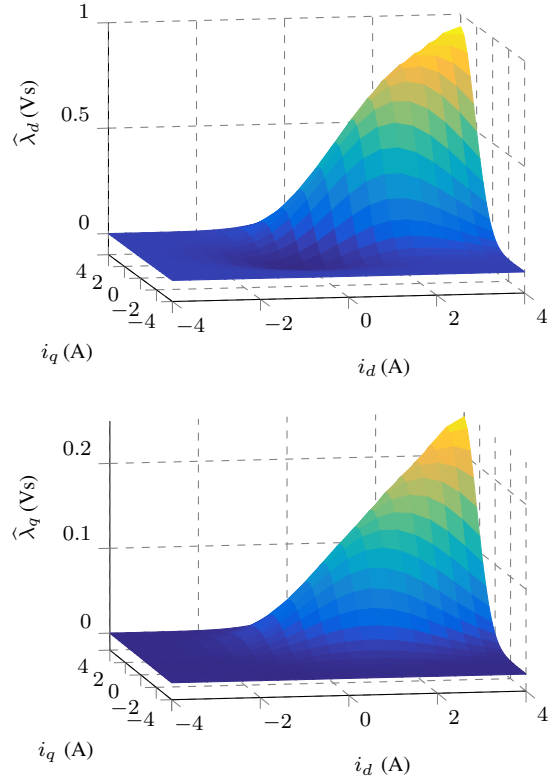


Fig. 6. RBF-based 3D magnetic maps, obtained by online training from blank conditions and sub-optimal MTPA strategy ( $i_d = i_q$ ).

To get an accurate flux linkages estimate, the stator resistance needs to be a known parameter. In the present work, an online tracking algorithm similar to that proposed by [20] was implemented. Essentially, it is based on a DC current injection over the  $\alpha$ -axis and allows the tracking of the resistance with high accuracy.

A first experiment was performed still out of the normal operations, in this case to explore the capability of the network to evolve from a completely blank situation. Six successive load torque steps (from 0 to the nominal torque  $T_N$ ) were imposed to the SynR motor by a virtual active load (Fig. 4), while the SynR motor was speed-controlled at a constant speed of 350 rpm. A simple sub-optimal ( $i_d = i_q$ ) current control strategy was selected, and the flux linkages estimation was activated at each step. In this way it was possible to investigate the local character of the RBF network. Fig. 6 shows the maps of  $\lambda_{dq}(i_d, i_q)$  after the six-step procedure. The local property of the network implies that all (and only) the weights close to the  $i_{dq}$  points are actually updated. As shown in Fig. 6, the estimated flux linkages are not null closely around the  $i_d = i_q$  line. However, the correctness of the estimation rapidly decrease as one deviates from the  $i_d = i_q$  line, due to incompleteness of the training for those points. In particular, the flux linkages estimation has not meaning below zero.

The effectiveness of the magnetic model obtained online was verified by comparing the estimated flux linkages of Fig. 6 with those obtained by the benchmark offline method [3] under the same operating conditions, i.e. along the line  $0 \leq i_d = i_q \leq I_N$ . The results are reported in Fig. 7.

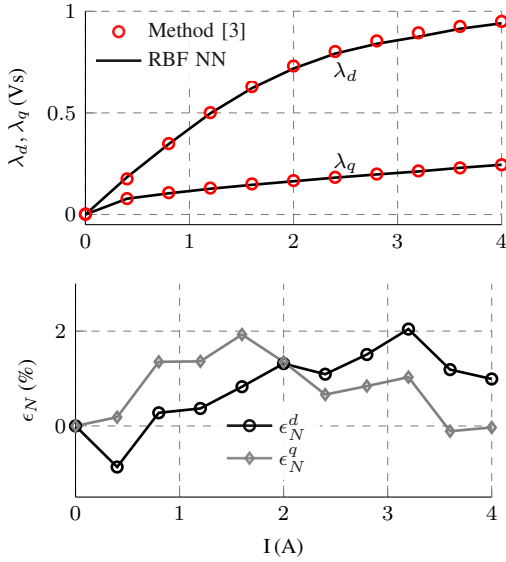


Fig. 7. Measured and estimated flux linkages along the  $45^\circ$  MTPA trajectory in the  $i_d$ - $i_q$  plane and the normalized errors.

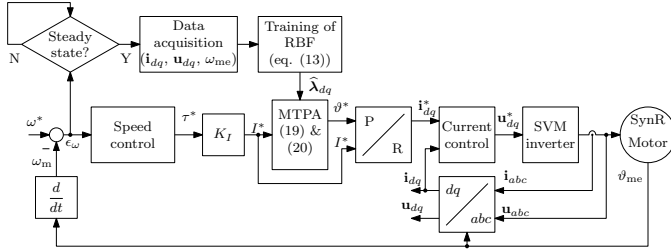


Fig. 8. Adaptive MTPA control of SynR motor by RBF network.

The errors still remain within a narrow band of 2%, except at very low currents ( $i_d = i_q \leq 0.1I_N$ ), where more neurons should be necessary. On the other hand, at such low values of current the SynR motor does not suffer of any saturation, so that a simple  $i_d = i_q$  current control is adequate.

### C. Online adaptive MTPA control

The last test carried out on the experimental setup was related to the identification of the real MTPA condition and its online tracking, based on the algorithm explained in Sect. IV. Thanks to the light training algorithm (13), the RBF network of Fig. 1 is continuously updated, so that an accurate and comprehensive magnetic model of the SynR motor is always available and it can be used to update the MTPA curve.

The procedure can be explained with the aid of Fig. 8. An outer speed control loop is usually present and it is supposed to produce the torque reference  $\tau^*$ . The torque reference is made proportional to the current reference amplitude  $I^*$ , by a constant  $K_I = T_N/I_N$  obtained from TABLE II. The phase voltages and currents  $\mathbf{u}_{abc}$ ,  $\mathbf{i}_{abc}$  are sampled at each control cycle and transformed into the synchronous reference frame by a Park transformation ( $dq/abc$ ). Their values are used to update the RBF-based flux linkages estimations  $\hat{\lambda}_{dq}$ . It is worth to remark that the RBF network weights were initialised supposing known and constant inductances  $L_d, L_q$

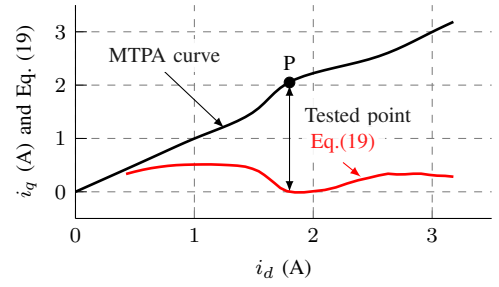


Fig. 9. Single MTPA point detection and output of (19) after the RBF training.

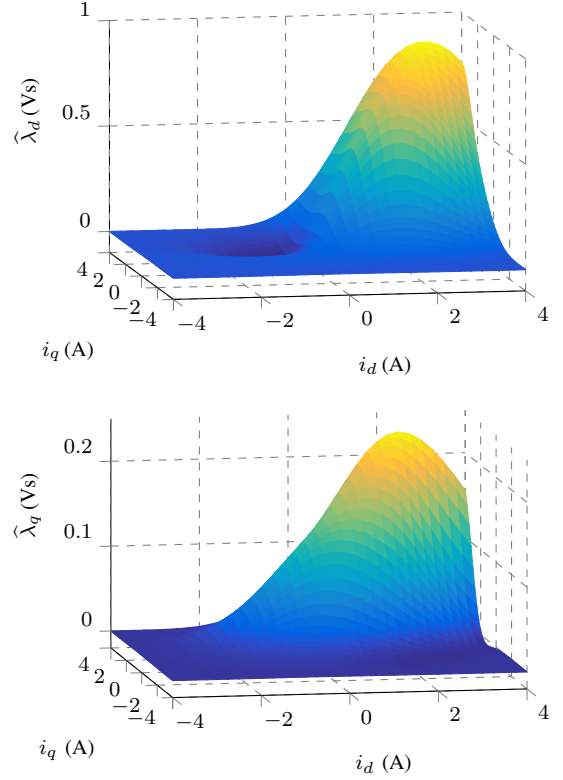


Fig. 10. 3D flux linkages maps after the convergence of the adaptive MTPA tracking procedure on five different working points (see text).

(TABLE II), so that the 3D plots  $\hat{\lambda}_d, \hat{\lambda}_q$  as function of currents were two simple inclined planes. The MTPA algorithm represented by (19) and (20) is then evaluated on the actual current request and the estimated flux linkages. The algorithm updates the phase  $\vartheta^*$  of the reference current vector, according to (19), first approaching and then maintaining the SynR motor drive in a dynamically updated MTPA condition. As an example, Fig. 9 reports the situation after the training in a single working point P. Should a transient occur, the MTPA curve would be the modified one. As testified by the output of (19), also reported in Fig. 9, the transient would be performed out of the MTPA condition except in the neighbourhood of point P. Over time, the RBF network will get completely trained and the MTPA trajectory detected by (19) will coincide with the true one. A polar-to-rectangular (P/R) transformation block returns the  $i_{dq}^*$  reference vector to the current control loop, which drives the inverter-fed SynR motor.

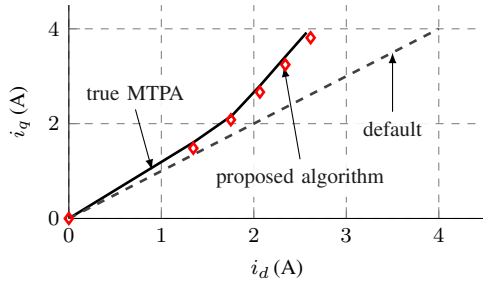


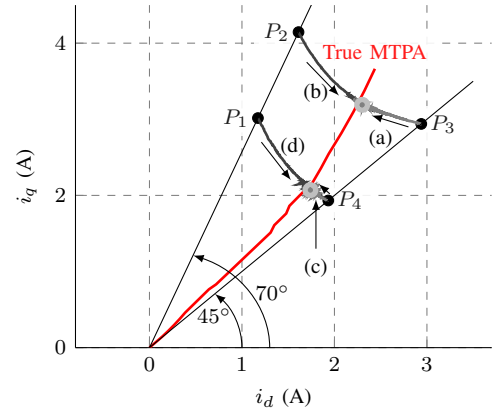
Fig. 11. MTPA points. The true MTPA was obtained offline by using a torque-meter.

The first experiment about adaptive MTPA was performed by applying five different load torque levels to the SynR motor drive. For each load torque level, i.e. at steady state, the adaptive MTPA algorithm ((19) and (20)) makes the current reference to leave the default  $i_d = i_q$  condition, by slightly modifying the phase  $\vartheta^*$  of the current vector itself. In parallel, a new set of RBF network weights are obtained by training the RBF network using the acquired voltages and currents. The new complete magnetic maps are reported in Fig.10.

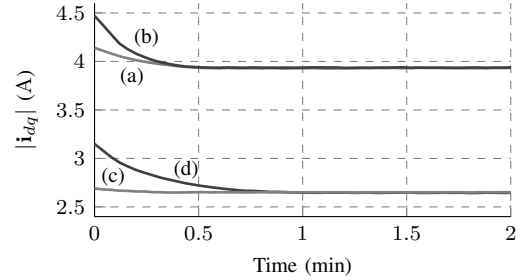
The five MTPA points reached by the adaptive algorithm are denoted by diamond-shaped marks in Fig. 11, which also reports as a solid line the real MTPA curve, obtained with offline measurements and the aid of a torque meter (which is not an option in the real application, of course). The dashed line refers to the initial default  $i_d = i_q$  condition. The accuracy is rather good, if one considers that it is obtained without any signal injection (and the related chattering problems). In this sense too, the proposed technique is innovative.

The MTPA condition (19) trusts on a correct flux linkages map. It takes time to the AC drive to get a well-trained RBF network in a sufficiently wide portion of the working plane. A second experiment was designed to evaluate the time needed to find a true MTPA point including the training of the RBF network. Anyway, in the real application it is worth noting that these two procedures (the RBF network training and the MTPA tracking) are independent, so that the former does not influence the dynamic of the latter. Thus, during torque transients the training is stopped and the MTPA condition is evaluated on the flux linkages map available at that moment.

The drive was started by imposing, with a virtual load, four different initial working points ( $P_{1,\dots,4}$  of Fig. 12a). Then, the adaptive MTPA algorithm described in the previous experiment was started. The real MTPA points were reached with the dynamic reported in Fig. 12b. The true MTPA curve in Fig. 12a was obtained with the aid of a torque-meter. The algorithm takes the current vector amplitude to its minimum, as shown in Fig. 12b. The convergence time can be reduced by processing the output of (19) with an additional regulator. This was not implemented because out of the scope of this work. Anyway, it is worth noting that the convergence is requested only once per point. After a while, the RBF network will get trained over the whole MPTA curve.



(a) MTPA search trajectories.



(b) Current amplitudes.

Fig. 12. Adaptive MTPA transient behaviour.

## VI. CONCLUSION

An accurate maximum torque per ampere control allows the minimisation of the copper losses, with the related benefits in terms of ac drive efficiency. This is particularly true for SynR motors, whose marked magnetic nonlinearity makes the usual  $i_d = i_q$  strategy quite imprecise. In this paper, a novel very light training algorithm made possible both the implementation and the online training of an RBF neural network. It has been found that the local property of the network makes it suitable for a precise flux linkages estimation and online tracking, starting from the measurement of motor currents and voltages. The availability of the magnetic model yielded the implementation of an adaptive MTPA control, without any signal injection. The experiments on a real SynR motor drive have clearly demonstrated the feasibility of the proposed control. To increase the reference value, mathematical insights and design hints have been included in the paper. They should help the implementation despite the complexity of the subject. A similar approach could be used for electric drives that require flux-weakening operations, by properly turning the MTPA condition (19) into a maximum torque-per-voltage condition.

## ACKNOWLEDGMENT

This work was supported by Fondazione Studi Universitari Vicenza.



## REFERENCES

- [1] M. Barcaro, N. Bianchi, and F. Magnussen, "Remarks on torque estimation accuracy in fractional-slot permanent-magnet motors," *IEEE Trans. Ind. Electron.*, vol. 59, no. 6, pp. 2565–2572, June 2012.
- [2] Z. Qu, T. Tuovinen, and M. Hinkkanen, "Inclusion of magnetic saturation in dynamic models of synchronous reluctance motors," in *2012 XXth International Conference on Electrical Machines*, Sept 2012, pp. 994–1000.
- [3] E. Armando, R. Bojoi, P. Guglielmi, G. Pellegrino, and M. Pastorelli, "Experimental identification of the magnetic model of synchronous machines," *IEEE Trans. Ind. Appl.*, vol. 49, no. 5, pp. 2116–2125, Sept 2013.
- [4] R. Dutta and M. F. Rahman, "A comparative analysis of two test methods of measuring  $d$ - and  $q$ -axes inductances of interior permanent-magnet machine," *IEEE Trans. Magn.*, vol. 42, no. 11, pp. 3712–3718, Nov 2006.
- [5] G. Pellegrino, B. Boazzo, and T. M. Jahns, "Magnetic model self-identification for PM synchronous machine drives," *IEEE Trans. Ind. Appl.*, vol. 51, no. 3, pp. 2246–2254, May 2015.
- [6] L. Ortombina, F. Tinazzi, and M. Zigliotto, "Magnetic modeling of synchronous reluctance and internal permanent magnet motors using radial basis function networks," *IEEE Trans. Ind. Electron.*, vol. 65, no. 2, pp. 1140–1148, Feb 2018.
- [7] Wanglei, X. Yunshi, W. Qidi, and Z. Guoxing, "Neural network based parameters identification and adaptive speed control of AC drive system," in *Industrial Technology, 1996. (ICIT '96), Proceedings of The IEEE International Conference on*, Dec 1996, pp. 118–121.
- [8] M. A. Rahman and M. A. Hoque, "On-line adaptive artificial neural network based vector control of permanent magnet synchronous motors," *IEEE Trans. Energy Convers.*, vol. 13, no. 4, pp. 311–318, Dec 1998.
- [9] J. Zhao and B. K. Bose, "Neural-network-based waveform processing and delayless filtering in power electronics and AC drives," *IEEE Trans. Ind. Electron.*, vol. 51, no. 5, pp. 981–991, Oct 2004.
- [10] M. A. Rahman, M. N. Uddin, and M. A. Abido, "An artificial neural network for online tuning of genetic algorithm-based PI controller for interior permanent magnet synchronous motor drive," *Canadian Journal of Electrical and Computer Engineering*, vol. 31, no. 3, pp. 159–165, Summer 2006.
- [11] T. Pajchrowski, K. Zawirski, and K. Nowopolski, "Neural speed controller trained online by means of modified RPROP algorithm," *IEEE Trans. Ind. Informat.*, vol. 11, no. 2, pp. 560–568, April 2015.
- [12] S. Haykin, *Neural Networks: A Comprehensive Foundation*. MacMillan Publishing Company, 1994.
- [13] N. Bedetti, S. Calligaro, C. Olsen, and R. Petrella, "Automatic MTPA tracking in IPMSM drives: Loop dynamics, design, and auto-tuning," *IEEE Trans. Ind. Appl.*, vol. 53, no. 5, pp. 4547–4558, Sept 2017.
- [14] F. J. Lin, Y. T. Liu, and W. A. Yu, "Power perturbation based MTPA with an online tuning speed controller for an IPMSM drive system," *IEEE Trans. Ind. Electron.*, vol. 65, no. 5, pp. 3677–3687, May 2018.
- [15] A. Dianov, K. Young-Kwan, L. Sang-Joon, and L. Sang-Taek, "Robust self-tuning MTPA algorithm for IPMSM drives," in *2008 34th Annual Conference of IEEE Industrial Electronics*, Nov 2008, pp. 1355–1360.
- [16] A. Consoli, G. Scarcella, G. Scelba, and A. Testa, "Steady-state and transient operation of IPMSMs under maximum-torque-per-ampere control," *IEEE Trans. Ind. Appl.*, vol. 46, no. 1, pp. 121–129, Jan 2010.
- [17] B. Cheng and T. R. Tesch, "Torque feedforward control technique for permanent-magnet synchronous motors," *IEEE Trans. Ind. Electron.*, vol. 57, no. 3, pp. 969–974, March 2010.
- [18] J. Lee, K. Nam, S. Choi, and S. Kwon, "Loss-minimizing control of PMSM with the use of polynomial approximations," *IEEE Trans. Power Electron.*, vol. 24, no. 4, pp. 1071–1082, April 2009.
- [19] G. Zanuso, L. Peretti, and P. Sandulescu, "Stator reference frame approach for DC injection-based stator resistance estimation in electric drives," in *2015 IEEE 11th International Conference on Power Electronics and Drive Systems*, June 2015, pp. 867–872.
- [20] R. Antonello, L. Ortombina, F. Tinazzi, and M. Zigliotto, "Online stator resistance tracking for reluctance and interior permanent magnet synchronous motors," *IEEE Trans. Ind. Appl.*, vol. 54, no. 4, pp. 3405–3414, July 2018.